Analysis on the Friction Losses of a Bent-Axis Type Hydraulic Piston Pump

Yeh-Sun Hong*, Yoon-Ho Doh

Hankuk Aviation University, School of Aeronautical & Mechanical Engineering, Hwajeon-dong, Duckyang-ku, Goyang-city, Gyeonggi-do, 412-791, Korea

The design of an axial piston pump for electro-hydrostatic transmission systems requires accurate information where and how much the internal friction and flow losses are produced. This study is particularly focused on the friction losses of a bent-axis type hydraulic piston pump, aiming at finding out which design factors influence its torque efficiency most significantly. To this end, the friction coefficients of the pump parts such as piston heads, spherical joints, shaft bearings, and valve plate were experimentally identified by a specially constructed tribometer. Applying the experimental data to the equations of motion for pistons as well as to the theoretical friction models for the pump parts, the friction torques produced by them were computed. The accuracy of the computed results was confirmed by the comparison with the practical input torque of the pump. In this paper, it is shown that the viscous friction forces on the valve plate and input shaft bearing are the primary source of the friction losses of the bent-axis type pump, while the friction forces and moments on the piston are of little significance.

Key Words : Bent-Axis Type Hydraulic Piston Pump, Kinematics Analysis, Dynamic Analysis, Friction Loss, Measurement of Friction Coefficients, Tribometer

Nomenclature

a_G : Acceleration of the mass center of a piston [m/s^2]
A_b : Effective pressurized area of cylinder bores [mm^2]
A_p : Piston head area [mm^2]
d_m : Mean diameter of bearing [mm]
F_A, F_B : Normal reaction forces on piston heads and spherical joints, respectively [N]
F_L : Load force on bearing [N]
F_f : Friction force on piston head [N]
m_P : Mass of a piston [kg]
M_{f_A}, M_{f_B} : Friction moments on piston heads and spherical joints, respectively [Nm]
N : Number of pistons
μ_v, μ_A, μ_B : Friction coefficients of valve plate, piston heads, and spherical joints, respectively
v : Kinetic viscosity of oil [cSt]
p_C : Cylinder chamber pressure [bar]
R_i, R_o : Internal and external radii of valve plate lands, respectively [mm]
r_i, r_o : Internal and external radii of valve plate ports, respectively [mm]
R_C : Rotation radius of cylinder bores relative to the cylinder barrel axis [mm]
R_S : Rotation radius of spherical joints relative to the input shaft axis [mm]
T_f^v, T_f^b : Friction torques on valve plate and bearings, respectively [Nm]
T_f^j, T_f^h : Friction torques generated by spherical joints and piston heads, respectively [Nm]
T_t : Total input torque [Nm]
$\vec{\omega}$, $\vec{\alpha}$: Angular velocity [rad/s] and accelera-

* Corresponding Author,
E-mail : yshong@hau.ac.kr
TEL : +82-2-300-0287; **FAX** : +82-2-3158-2191
Hankuk Aviation University, School of Aeronautical & Mechanical Engineering, Hwajeon-dong, Duckyang-ku, Goyang-city, Gyeonggi-do, 412-791, Korea. (Manuscript **Received** January 9, 2004; **Revised** May 27, 2004)

tion of piston [rad/s^2], respectively

θ_S, ω_S : Input shaft angle [deg] and input shaft speed of pump [rpm], respectively

V_A, V_B : Velocities of pistion heads and spherical joints, respectively [m/s]

XYZ : Global coordinate system with the origin on input shaft

X'Y'Z' : Local coordinate system with the origin on cylinder barrel

1. Introduction

Recently, a series of innovative attempts to replace the conventional Fly-by-Wire systems of aircrafts by the so-called Power-by-Wire systems have been made by aircraft makers, aiming at eliminating heavy and complex hydraulic pipes connecting main pumps and each electro-hydraulic actuators (Sutton, 1997 ; N. N., 2001). Therefrom, it is expected that the fuel consumption and the maintenance cost of the aircrafts are reduced, while the pay load is increased.

The Power-by-Wire system bases on a new kind of electro-hydraulic actuators which are supplied with electrical power instead of hydraulic one. They consist of a constant displacement pump and a hydraulic cylinder forming a closed circuit, where the pump is driven by an electrical servomotor whose angular velocity is controlled to position the hydraulic cylinder. In this way, any flow control devices for the position control such as servo-valves generating the power loss by flow restriction, are saved. Therefore, they are called as electro-hydrostatic actuators (abbreviated as EHA in the following) in order to distinguish them from the conventional valve-controlled type.

In concern with the pumps for the EHA, they should be small to save the space and weight. It means that they should operate at high speed, simultaneously satisfying the general requirements on the operation efficiency and the working pressure. And they should also allow the dynamic change of the angular velocity to accurately compensate the position control error.

These conditions can be most advantageously met by the bent-axis type piston pumps which use timing gears to connect the input shaft with the cylinder barrel. Their pistons are almost free from lateral forces affecting the wear and friction between themselves and cylinder bores. These pumps generally have max. operation pressure higher than 350 bar. And, in case of small-sized types, they can operate at the rotational speed up to 10,000 rpm.

In order to design a highly efficient, high-speed and small-sized pump for the EHA, it is necessary to know which design factors significantly influence its friction losses and flow leakage. In this study, the scope will be bounded to the friction loss analysis.

As for the swash-plate type piston pumps, a lot of studies have been made to investigate the tribological phenomenon on the pistons, slipper pads, and valve plates (Darling, 1985 ; Ezato, 1986 ; Iboshi, 1986 ; Kobayashi, 1988 ; Matsumoto, 1991 ; Kobayashi, 1993 ; Olems, 2002), their effects on the input shaft torque (Manring, 1998), and the dynamics of the swash plate control related with the reciprocating motion of pistons (Zeiger, 1985 ; Schoenau, 1990 ; Cho, 2000), since they have been widely applied not only as constant flow pump, but also as pressure- or power-compensated pump with moderate dynamic response. It comes from that their volumetric displacement can be simply changed by the tilt motion of the swash plate.

In contrast with that, few studies have been focused on the bent-axis type piston pumps. As constant flow pump operating under 4,000 rpm they are very reliable and efficient. But their volumetric displacement control for pressure- or power-compensation is only allowed to relatively slow processes because the dynamic inclination angle change of their cylinder barrel has to overcome large inertial and mechanical resistance. Therefore, the study on their dynamics and tribological problems raised by the spatial motion of the pistons has not been strongly motivated until now.

But if we have to design a EHA pump whose volumetric displacement is smaller than 3c.c./rev and max. rotational speed higher than 10,000 rpm, it is essential to know how and how much

the high-speed spatial piston motion produces the reaction and friction forces on the piston heads, spherical joints, shaft bearings, and valve plate. Here, the surface conditions of these components play a significant role.

Doh and Hong (2002) derived the kinematic and dynamic equations of the piston motion of a bent-axis type piston pump, and solved them to compute the friction forces produced by the pistons and valve plate, where the information on the practical friction coefficients was not completely available. Therefore, the experimental evaluation of the computed results has remained to be done.

In this study, the kinematics and dynamics of the spatial piston motion will be briefly explained, defining the friction models for the piston heads and spherical joints. The friction coefficients of the piton heads, spherical joints, valve plate, and shaft bearing were experimentally identified using a specially constructed tribometer so that the estimation error of the friction losses can be minimized. The test method will be described, referring to the theoretical friction models of valve plate and shaft bearing.

Finally, based on the experimentally confirmed friction models of the pump parts, their effects on the friction loss of the object pump were investigated. In order to examine the accuracy of the friction loss analysis, the torque efficiency of a bent-axis piston pump was measured and compared with the computed value. They showed good agreement. This paper is concluded with the discussion how the friction losses at low and high input shaft speed range can be minimized.

2. Kinematics of the Piston Motion

The bent-axis type piston pump investigated in this paper connects its cylinder barrel with the input shaft by bevel gears, as shown in Fig. 1. Its basic specifications are summarized in Table 1. The pump components subjected to friction losses are the shaft bearings, bevel gears, spherical joints, piston heads, and valve plate. For the friction loss analysis of the pump, their relative sliding velocities for a given input shaft speed

Table 1 Basic specifications of object pump

Volumetric displacment	4.88 cc/rev
Cylinder bore diameter	9.5 mm
No. of pistons	5
Pistion stoke	13.77 mm

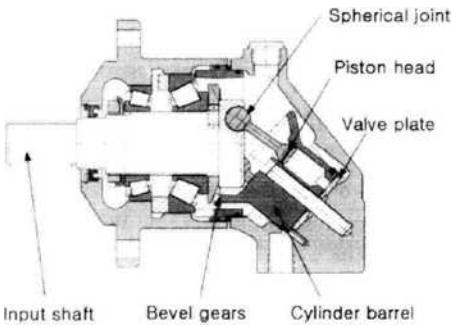

Fig. 1 Structure of a bent-axis type piston pump with bevel gears as coupling device

should be known. In case of the piston heads and spherical joints, the kinematic analysis of the spatial piston motion is required, whereas the rotational speeds of the shaft bearings, bevel gears, and cylinder barrel are directly given by the input shaft.

Figure 2 shows the important parameters and their actual values for the kinematic analysis in this study.

Relative to the Cartesian coordinate system XYZ with its origin located at O on the center of the drive flange, the absolute velocity vector of a piston head, $\vec{V}_A$, and that of a spherical joint, $\vec{V}_B$, are related by

$$\vec{V}_B = \vec{V}_A + \vec{\omega} \times \vec{R}_{BA} \tag{1}$$

where $\vec{\omega}$ denotes the angular velocity vector of the piston body and $\vec{R}_{BA}$ the position vector of the spherical joint relative to the piston head. Assuming that the piston does not rotate along its longitudinal axis, we obtain an additional equation : i.e.

$$\vec{\omega} \cdot \vec{R}_{BA} = 0 \tag{2}$$

From equations (1) and (2), $\vec{\omega}$ and the piston head velocity relative to the cylinder bore, $\vec{V}'_A$, can be solved for given $\vec{V}_B$. And the time

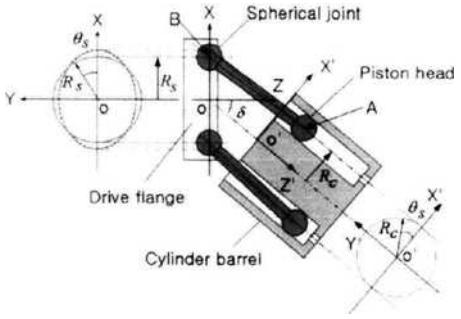

Inclination angle of cylinder barrel, δ	40 deg
Rotating radius of spherical joints, R_S	10.75 mm
Rotating radius of cylinder chambers, R_C	9.5 mm

(a) Coordinate systems and important kinematic parameters

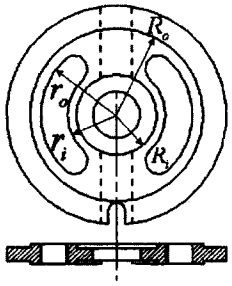

R_I	6.25 mm	r_I	7.4 mm
R_O	13.25 mm	r_O	11.6 mm

(b) Shape of valve plate

Fig. 2 Kinematic parameters of object pump

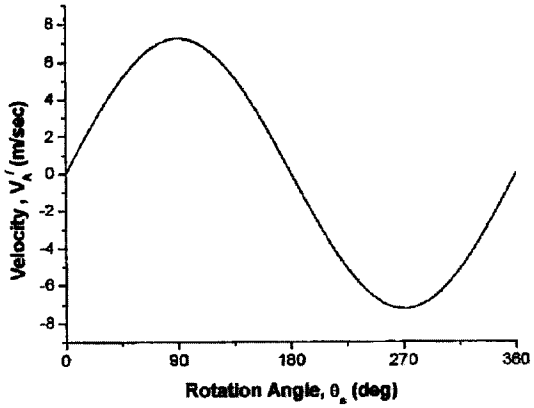

(a) Piston head velocity

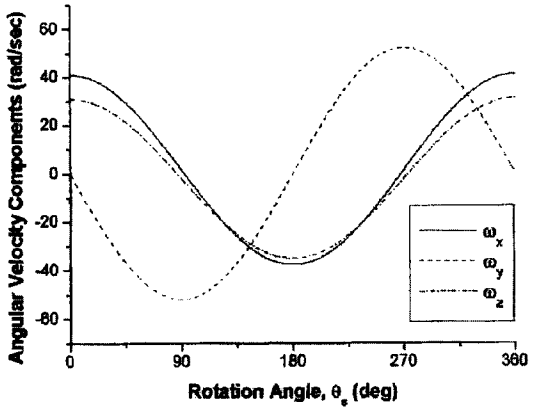

(b) Angular velocity components of piston

Fig. 3 Translation and rotation velocities of piston (ω_S=10,000 rpm)

derivative of eqs. (1) and (2), respectively, gives two equations for solving the angular acceleration of the piston body, $\vec{\alpha}$, and the piston head acceleration for given $\vec{a}_B$. For more details the study of (Doh and Hong, 2002) is to be referred.

As an important result of the kinematic analysis, Fig. 3 shows the piston head velocity relative to the cylinder bore, $\vec{V}_A'$, and the angular velocity components of the piston body as function of input shaft angle when the input shaft speed is 10,000 rpm. The max. velocity of the piston head turned out to be approximately 7 m/s, while the piston body rotates with the max. angular velocity of about 50 rad/s. As the radius of the spherical joints is 5.5 mm, the sliding velocity of their internal contact surfaces is not higher than 0.275 m/s.

3. Dynamics of the Piston Motion

In order to compute the friction forces generated by the pistons making translational and rotational motions relative to the cylinder bore axes, their equations of motion can be derived from the free body diagram illustrated in Fig. 4.

Here the axial load, F_p, produced by the cylinder chamber pressure, p_C, is the function of input shaft angle.

F_{Bx}, F_{By} and F_{Bz} are the reaction force components on the spherical joint in terms of the

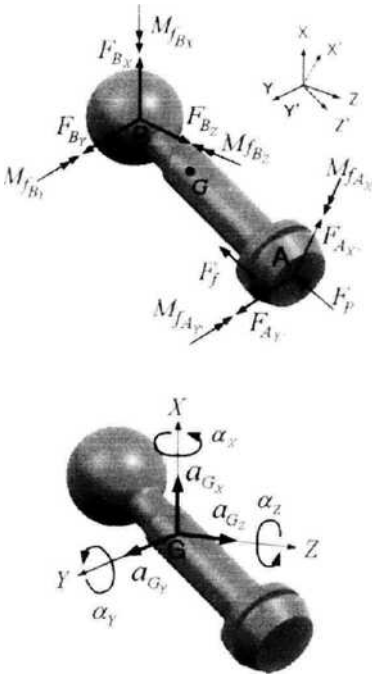

Fig. 4 Free-body diagram of piston

XYZ-coordinate system. The friction moment, $\vec{M}_{f_B}$, generated on the spherical joint is determined by the reaction force, $\vec{F}_B$, friction coefficient, μ_B, and radius, R_B, while its direction is opposite to $\vec{\omega}$. Its Cartesian components are expressed by

$$M_{f_{B_X}}=\frac{-\omega_X}{\sqrt{\omega_X^2+\omega_Y^2+\omega_Z^2}}R_B\mu_B\sqrt{F_{B_X}^2+F_{B_Y}^2+F_{B_Z}^2}$$

$$M_{f_{B_Y}}=\frac{-\omega_Y}{\sqrt{\omega_X^2+\omega_Y^2+\omega_Z^2}}R_B\mu_B\sqrt{F_{B_X}^2+F_{B_Y}^2+F_{B_Z}^2} \quad (3)$$

$$M_{f_{B_Z}}=\frac{-\omega_Z}{\sqrt{\omega_X^2+\omega_Y^2+\omega_Z^2}}R_B\mu_B\sqrt{F_{B_X}^2+F_{B_Y}^2+F_{B_Z}^2}$$

Similarly, $F_{A_{X'}}$ and $F_{A_{Y'}}$ are the reaction force components on the piston head relative to the X'Y'Z'-coordinate system with its origin located at O' on the rotation axis of the cylinder barrel. The friction force, $\vec{F}_f$, proportional to the reaction force, $\vec{F}_A$, acts on the X'Y'-plane in the opposite direction of $\vec{V}'_A$. The friction force and the Cartesian components of the friction moment can be expressed as

$$F_f=\frac{-V'_A}{|V'_A|}\mu_A\sqrt{F_{A_{X'}}^2+F_{A_{Y'}}^2} \quad (4)$$

$$M_{f_{A_{X'}}}=\frac{-V'_A}{|V'_A|}\mu_A R_A F_{A_{X'}}$$
$$M_{f_{A_{Y'}}}=\frac{V'_A}{|V'_A|}\mu_A R_A F_{A_{Y'}} \quad (5)$$

where R_A denotes the radius of the piston head.

The equations of motion for the piston can be expressed by eqs. (6) and (7) in terms of the XYZ-coordinate system. Here the Cartesian components of the external forces and moments are to be induced from the free body diagram in Fig. 4.

$$\sum F_X=m_P a_{G_X},\ \sum F_Y=m_P a_{G_Y},\ \sum F_Z=m_P a_{G_Z} \quad (6)$$

$$\begin{aligned}\sum M_{G_X}&=I_X\alpha_X-(I_Y-I_Z)\omega_Y\omega_Z+I_{XY}(\omega_Z\omega_X-\alpha_Y)\\&\quad -I_{YZ}(\omega_Y^2-\omega_Z^2)-I_{ZX}(\omega_X\omega_Y+\alpha_Z)\\\sum M_{G_Y}&=I_Y\alpha_Y-(I_Z-I_X)\omega_Z\omega_X+I_{YZ}(\omega_X\omega_Y-\alpha_Z)\\&\quad -I_{ZX}(\omega_Z^2-\omega_X^2)-I_{XY}(\omega_Y\omega_Z+\alpha_X)\\\sum M_{G_Z}&=I_Z\alpha_Z-(I_X-I_Y)\omega_X\omega_Y+I_{ZX}(\omega_Y\omega_Z-\alpha_X)\\&\quad -I_{XY}(\omega_X^2-\omega_Y^2)-I_{YZ}(\omega_Z\omega_X+\alpha_Y)\end{aligned} \quad (7)$$

where I_X, I_Y, I_Z, I_{XY}, I_{YZ}, I_{XZ} are the moments and the products of inertia about the mass center G. The acceleration of the mass center, $\vec{a}_G$, can be obtained from $\vec{\omega}$, $\vec{\alpha}$, and $\vec{a}_B$ by

$$\vec{a}_G=\vec{a}_B+\vec{\alpha}\times\vec{R}_{GB}+\vec{\omega}\times(\vec{\omega}\times\vec{R}_{GB}) \quad (8)$$

where $\vec{R}_{GB}$ denotes the position vector of the mass center relative to the spherical joint.

4. Experimental Identification of Friction Models for Pump Parts

4.1 Tribometer

The friction coefficients of the pump parts such as spherical joints, valve plate and shaft bearings are dependent on the material properties as well as its surface treatment conditions. For their identification a tribometer was constructed whose working principle was originally proposed by Siebel and Kehl (Murrenhoff, 2002). This kind of tribometer has been widely applied to simulate the tribological phenomenon between sliding surfaces of various mechanical components. It's basic configuration is schematically shown in Fig. 5. While the upper disk is fixed to the

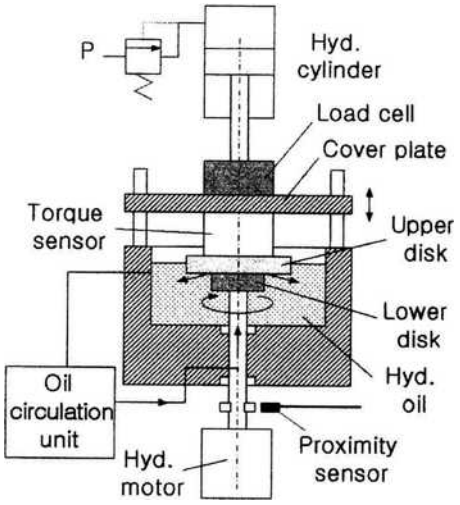

Fig. 5 Configuration of tribometer

reaction torque sensor which is mounted on the cover plate constrained to the vertical movement, the lower one is rotated by a hydraulic motor. The rotational speed of the hydraulic motor is monitored using a proximity sensor and a pair of teeth built on the drive shaft.

The two disks have ring-shaped contact surfaces and their contact force can be changed by the hydraulic cylinder whose extension force is regulated by a adjustable pressure control valve. The actual normal force is measured by a load cell located between the piston rod and the cover plate. In this way, the friction torque generated on the contact surfaces of the two disks, the normal force and the rotational speed are simultaneously measured.

Through the drive shaft of the lower disk, oil is supplied to the contact surfaces to lubricate them and flush out wear particles. It is circulated by a pump and continuously filtered, while its temperature is regulated to a preset value. The hydraulic cylinder can develop a contact pressure up to 2.5 N/mm^2 on the contact surfaces of the disks, whereas the hydraulic motor can rotate up to 10,000 rpm.

4.2 Friction model for valve plate

The friction torque between the cylinder barrel and the valve plate, T_f^V, which is dependent on the pressure variation of each cylinder chambers can be mathematically expressed as (Cho, 2000)

$$T_f^V=\left[\sum_{i=1}^{N}A_b p_{c_i}\right]\mu_V R_C \tag{9}$$

where N= number of pistons, $A_b=A_p-\frac{\pi}{2N}\left\{\frac{(R_o^2-r_o^2)}{\ln(R_o/r_o)}-\frac{(R_i^2-r_i^2)}{\ln(R_i/r_i)}\right\}$ and R_C denotes the mean radius of R_o and R_i.

Since the pump in this study has 5 pistons, the cylinder chambers have an angular interval of 72°. Eq. (9) denotes that the normal force generating the friction torque on the valve plate is the sum of the forces produced by each cylinder chamber pressure, p_{c_i}, acting on the effective area of the cylinder barrel, A_b. As the 5 cylinder chambers cross over the inlet and outlet ports of the valve plate one after another, their individual pressure waveform having an identical pattern with suction and discharge pressure regions will be sequentially shifted by 72° with respect to input shaft angle.

The friction coefficient, μ_V, represents the coulomb and viscous friction. The coulomb friction part can be quantified by only experimental measurement using the tribometer described above. For this measurement, the two disks were replaced by actual valve plate and cylinder barrel.

On the contrary, the viscous friction part can be theoretically expressed, the two pump parts being considered as circular rings. Hereat, it was assumed that the clearance between the cylinder barrel and the valve plate is constant and the oil flow there is primarily oriented in the radial direction.

Figure 6 shows the measured coulomb friction data and the computed viscous friction curve, where the clearance between the cylinder barrel and the valve plate was assumed to be 10 μm, as generally accepted. The oil viscosity was 70 cSt. Summing them, we obtain the total friction coefficient curve as shown in Fig. 7. In Fig. 6 the measured data are not given between 0 and 200 rpm because the stick-slip phenomena made it impossible to continuously change the rotational speed of the cylinder barrel in this speed range.

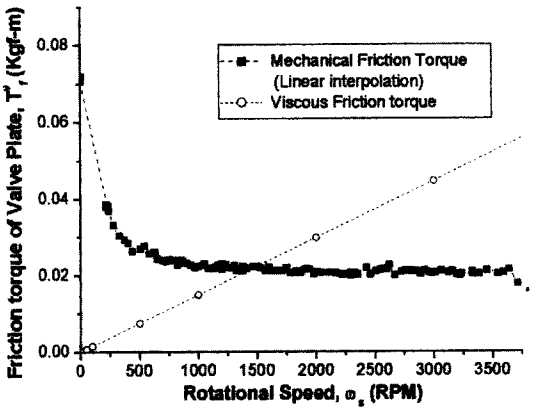

Fig. 6 Coulomb and viscous friction torques between cylinder barrel and valve plate

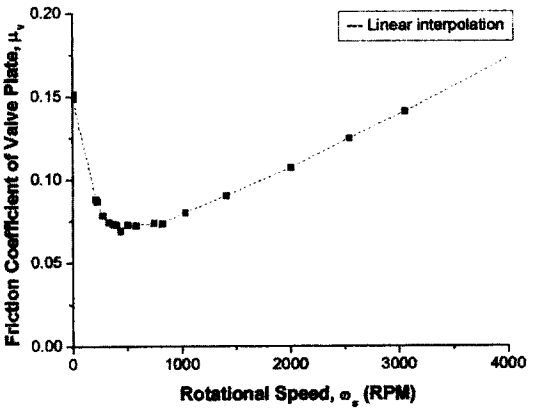

Fig. 7 Total friction coefficient between cylinder barrel and valve plate

4.3 Friction model for shaft bearings

Palmgren derived an empirical equation to mathematically express the friction torque on the shaft bearing as following (Tedric, 2001):

$$T_f^b = T_m + T_v \tag{10}$$

where

T_m=mechanical friction torque=$f_1 F_L^a d_m^b$

T_v=viscous friction torque

$$= \begin{cases} 10^{-7} f_0 (v\omega_S)^{2/3} d_m^3 & (\text{if } v\omega_S \geq 2000) \\ 160 \times 10^{-7} f_0 d_m^3 & (\text{if } v\omega_S < 2000) \end{cases}$$

The coefficients f_1, f_0, a and b are given by bearing makers (SKF, 2003). Using eq. (10), T_f^b was computed and compared with the measured

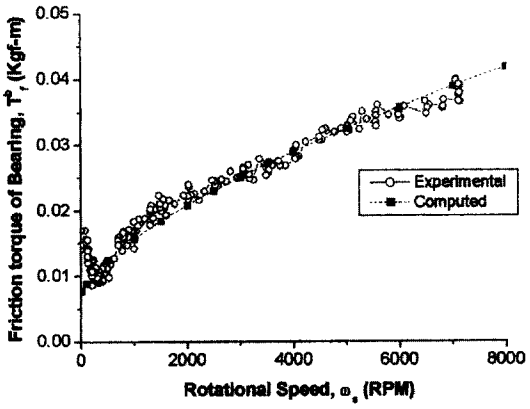

Fig. 8 Friction toque produced by shaft bearing

data which were obtained by the tribometer. Here the two disks were also replaced by the inner and outer race of an actual shaft bearing. Fig. 8 shows the results. It can be seen that eq. (10) is quite accurate.

4.4 Friction model for piston head and spherical joint

The friction force and friction moments generated on the piston head and the spherical joint are previously expressed by eqs. (3), (4) and (5). Since the piston heads and the spherical joints are made of same material and have same surface quality, they have same friction coefficient. In order to experimentally identify its value using the tribometer, two ring-type specimen having same material property and surface condition were used.

Figure 9 shows the measured results. The experiment under the tangential speed of 0.7 m/s was not possible because of the stick-slip phenomenon. However, the friction coefficient in the low speed range can be assumed by linear interpolation between 0.04 and 0.09, the static friction coefficient.

As mentioned above, the spherical joint makes slide motion on its surface with the velocity lower than 0.3 m/s even at the max. input shaft speed of 10,000 rpm. It can be seen that its friction coefficient changes between 0.07 and 0.09 within this speed range.

In case of the piston head, its translational

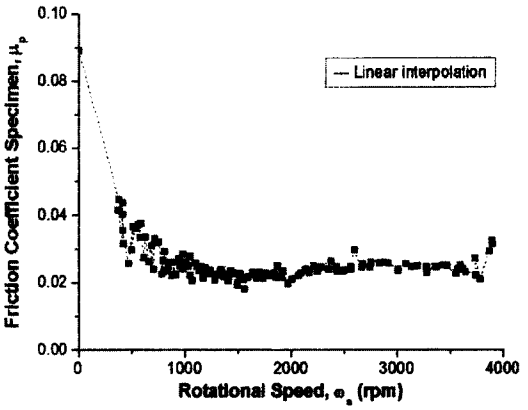

Fig. 9 Friction coefficient of specimen representing spherical joint and piston head

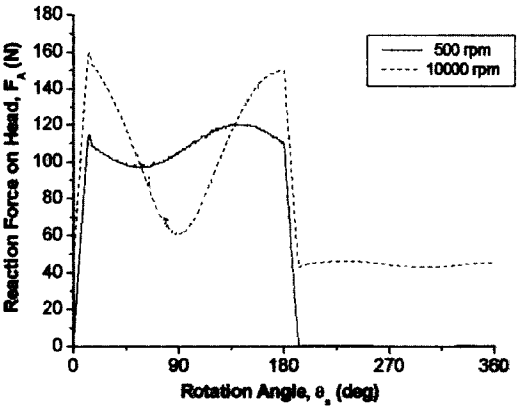

Fig. 10 Change of normal reaction force on a piston head

speed reaches up to 7 m/s when the input shaft rotates at 10,000 rpm. As explained later again, the reaction force on the piston head, F_A, is smaller than 160 N, whereas that on the spherical joint, F_B, is as large as 2,150 N. Therefore, the friction coefficient of the piston head can be roughly assumed as 0.02 without significantly affecting the modeling accuracy.

5. Results of Friction Loss Analysis

Using the friction coefficients identified as described above, the normal reaction force on the piston heads, F_A, and that on the spherical joints, F_B, were computed. Fig. 10 and 11 depict the results as function of input shaft angle at the rotational speed of 500 and 10,000 rpm, respectively, where a load pressure of 300 bar was applied. Concerning the dynamic pressure variation in each cylinder chamber, it was assumed to change as shown in Fig. 12. This pressure waveform was obtained by separate computer simulation with the valve plate geometry shown in Fig. 2 applied. It differs from the practical data in respect that the pressure pulsation at the pump outlet is not represented during the discharge stroke.

As the input shaft speed increases, F_A is mostly affected by the inertial force because the angular acceleration of the piston gets progressively larger. But its magnitude is still smaller

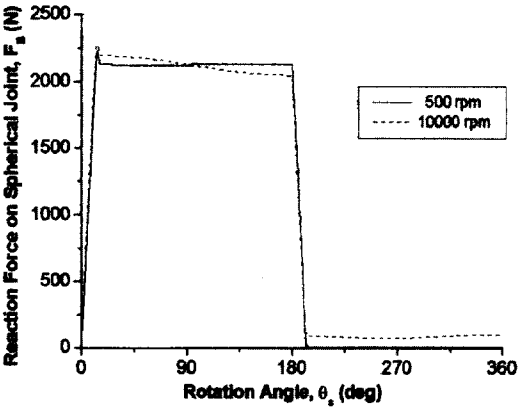

Fig. 11 Change of normal reaction force on a spherical joint

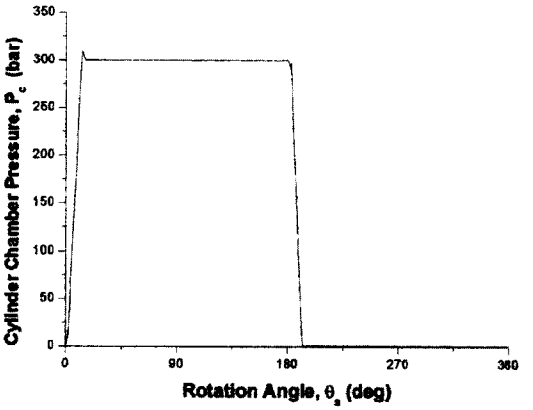

Fig. 12 Reference pressure waveform of each cylinder chamber

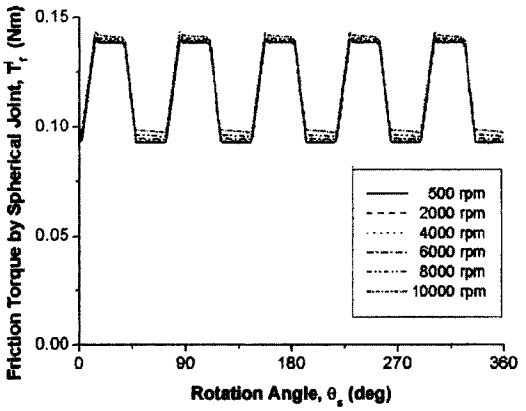

Fig. 13 Change of friction torque generated by spherical joints

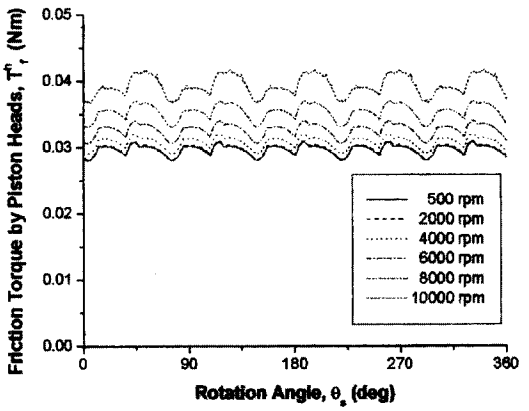

Fig. 14 Change of friction torque generated by piston heads

than 160 N. In contrast with that, F_B, mainly dependent on the cylinder chamber pressure, p_C, is less influenced by the input shaft speed.

Once the friction force and the friction moments on the pistons have been obtained from the dynamic analysis, the required input torque to overcome them can be computed by applying the work and energy method.

Figure 13 shows the friction torque generated by spherical joints, T_f^j, as function of input shaft angle with the input shaft speed changed as parameter. It can be seen that they result in the increase of the required input torque by an average value of 0.12 Nm at ω_S=10,000 rpm when the pump is loaded with 300 bar. Although the normal reaction force on the spherical joints, F_B, is as high as 2,150 N under this operation condition, the friction moment, M_{fB}, is inherently low because the friction coefficient is smaller than 0.025, as illustrated in Fig. 9. As the object pump has 5 pistons, T_f^j ripples 5 times during 1 revolution of the input shaft.

Since a theoretical input torque of 23.83 Nm is required to drive the pump with the volumetric displacement of 4.99 cc/rev at the load pressure of 300 bar, the friction torque generated by the spherical joints equals to approximately 0.5% of it.

As shown in Fig. 14, the additional input torque caused by the friction forces on the piston heads, T_f^h, under the same operation condition is smaller than 0.04 Nm at ω_S=10,000 rpm. Therefore, the piston heads turned out to have least influence on the friction loss. It is to be noted that the waveform of T_f^h is quite different from T_f^j, T_f^v, and T_f^v as shown below. Fig. 13 and Fig. 14 indicate that the required input torques caused by the friction forces on the spherical joints and piston heads are little dependent on the input shaft speed, whereas they are proportional to the load pressure in principle.

If the measured value of the friction coefficient, μ_V, in Fig. 7 is substituted into eq. (9), the friction torque generated between the cylinder barrel and the valve plate, T_f^v, equals to 0.191 Nm at ω_S=500 rpm and to 1.64 Nm at ω_S=10,000 rpm, as shown in Fig. 15 when the pump is loaded with 300 bar. It means that the viscous friction on the valve plate increases the required input torque up to approximately 7% of the theoretical input toque.

If the friction torque generated by the shaft bearing, T_f^b, is computed by eq. (10) for the same operation conditions, the results indicate the increase of the required input torque by 0.91 Nm, about 3.8% of the theoretical input toque, at ω_S=10,000 rpm (Fig. 16).

Finally, it can be noted that the friction torque of the object pump is mainly produced by the valve plate and shaft bearing. The friction forces on the piston heads and spherical joints turned out to have little influence on the friction loss

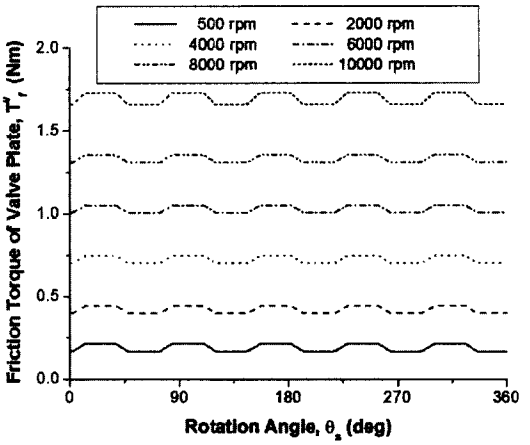

Fig. 15 Change of friction torque generated by valve plate

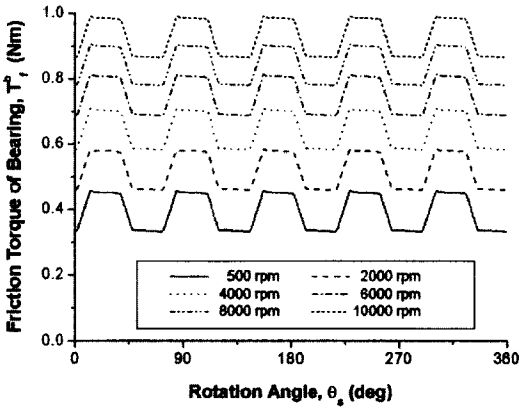

Fig. 16 Change of friction torque generated by shaft bearing

even at the high shaft speed of 10,000 rpm.

If the friction torques generated by the piston heads, spherical joints, valve plate and bearing are summed together, it amounts about 2.6 Nm at ω_S=10,000 rpm at the load pressure of 300 bar. It corresponds to 10.9% of the theoretical input torque. The total input torque, T_t, obtained by superposing the friction torques to the theoretical input torque, is given by Fig. 17.

In order to examine the analysis error of the friction loss, the practical input torque was measured and compared with the computed value. Figure 18 shows the results, where the load pressure was set to 68 bar (1,000 psi) and 136 bar

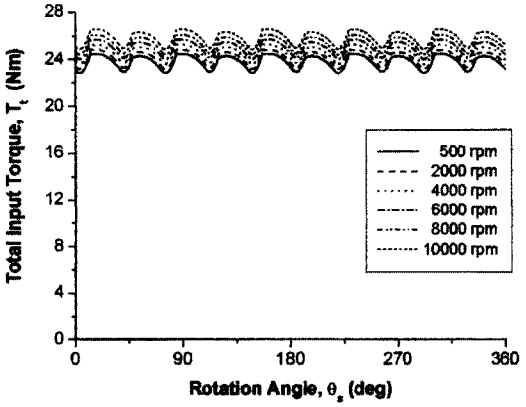

Fig. 17 Total input torque at load pressure=300 bar

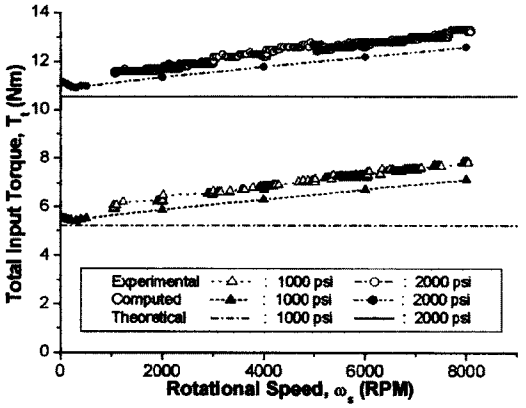

Fig. 18 Comparison of computed total input torque with experimental data

(2,000 psi), respectively. The computed total input torques are slightly smaller than the measured ones. The maximum error between them amounts approximately 6%, if it is defined as

$$\frac{(\text{computed value}-\text{measured value})}{\text{measured value}}\times 100$$

This error may be caused by the assumption that the clearance between the cylinder barrel and the valve plate has an average value of 10 μm and that the friction torque of the bevel gears is negligible. If the mechanical efficiency of the bevel gears ranging from 98% to 99% is taken into consideration (Townsend, 1992), the error could be even smaller.

Because of the stick-slip effect occurring at the pump drive unit, the object pump could not be

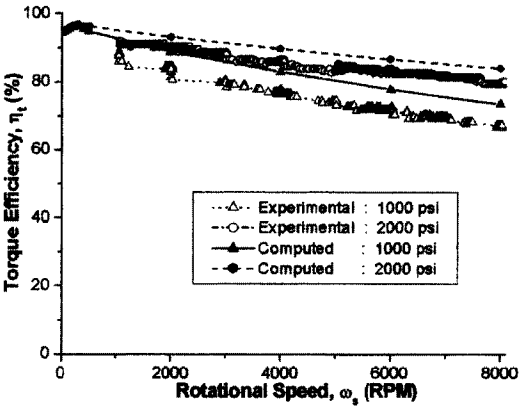

Fig. 19 Torque efficiency of object pump

tested in the input shaft speed range between 0 and 1,000 rpm.

Fig. 19 shows the same results in terms of the torque efficiency. The object pump indicated a practical torque efficiency of about 85% at ω_S= 4,000 rpm and 75% at ω_S=8,000 rpm for the load pressure of 136 bar.

As mentioned above, the friction torque of the object pump is mainly produced by the valve plate and shaft bearing. Their viscous frictions play a significant role as the input shaft speed increases. And Fig. 18 indicates that their coulomb friction part will increase the starting torque by approximately 3.7% of the theoretical input torque when the load pressure is 136 bar. This may cause the stick-slip motion of the pump when it should creep or run slowly at high load pressure. While the viscous friction can be reduced by their rotation radius, the coulomb friction may be suppressed by proper treatment of sliding surfaces.

6. Conclusions

The friction loss analysis in this study indicated that the friction torque of a bent-axis type piston pump is mainly produced by the valve plate and input shaft bearing. In contrast to that, the friction forces and moments on the pistons including spherical joints turned out negligibly small.

The analysis error in this study may have mainly resulted from the assumption that the clearance between the cylinder barrel and valve plate has a constant value of 10 μm. As future work, this parameter should be experimentally investigated to improve the modeling accuracy. Furthermore the friction characteristics of the piston head with seal rings should be studied, and their surface roughness should be considered as well. (Kim, 2002)

According to the study, the diameters of the valve plate and the shaft bearing should be minimized in order to increase the torque efficiency of the object pump at high input shaft speed.

Apart from the friction losses dependent on the input shaft speed, the coulomb friction of the valve plate may be the main reason for the dead band when the input shaft speed of the pump should be precisely controlled to position the hydraulic cylinder of an EHA. The coulomb friction of the valve plate is to be reduced by an improved treatment of the cylinder barrel's bottom surface mating with it.

Therefore, reshaping the valve plate, improving the surface condition of the cylinder barrel, and changing the shaft bearing arrangement should be studied further so that the pump can be advantageously applied to the electro-hydrostatic transmission control.

Acknowledgment

Authors are gratefully acknowledging the financial support by Korea Aerospace Technology Research Association of Ministry of Commerce, Industry and Energy and the cooperative research support by Hanwha, Co.

References

Cho, J. H., 2000, "Dynamic Modeling and Analysis for Swash-Plate Type Axial Pump Control Utilizing Indexing Valve Plate," Ph. D. Thesis, Univ. of Missouri-Columbia.

Darling, J., 1985, "Piston-Cylinder Dynamics in Oil Hydraulic Axial Piston Pumps," Ph. D. Thesis, School of Mechanical Engineering, University of Bath, England.

Doh, Y. H. and Hong, Y. S., 2002, "Dynamic Analysis of the 3-Dimensional Piston Motion of a Bent-Axis Type Hydraulic Pump," *Proceedings of the KAMES 2002 Joint Symposium*, Vol. A, pp. 861~867.

Ezato, M. and Ikeya, M., 1986, "Sliding Friction Characteristics between a Piston and a Cylinder for starting and Low-Speed Conditions in the Swashplate-Type Axial Piston Motor," *Proc. 7th Int. Fluid Power Symposium*, Bath, England.

Iboshi, N. and Yamaguchi, A., 1986, "Characteristics of a Slipper Bearing for Swash-Plate Type Axial Piston Pumps and Motors," *J. JSME*, Vol. 29, No. 254, pp. 2539~2546.

Kim, J. Y., Kim J. W., Cho, M. R. and Han, D. C., 2002, "Friction Characteristics of Piston Ring Pack with Consideration of Mixed Lubrication : Parametric Investigation," *Int. J. KSME*, Vol. 16, No. 4, pp. 468~475.

Kobayashi, S. and Matusmoto, K., 1993, "Lubrication between the Valve Plate and Cylinder Block for Low-Speed Conditions in a Swash-Plate Type Axial Piston Motor," *J. JSME*, Vol. 59, No. 561, pp. 1512~1517.

Kobayashi, S., Hirose, M., Hatsuse, J. and Ikeya, M., 1988, "Friction Characteristics of a Ball Joint in the Swash-Plate Type Axial Piston Motor," *Proc. 8th Int. Fluid Power Symposium*, Birmingham.

Manring, N. D., 1998, "The Torque on the Input Shaft of an Axial-Piston Swash-Plate Type Hydrostatic Pump," *J. Dynamic Systems*, Measurement, and Control, Vol. 120, pp. 57~62.

Matsumoto, K. and Ikeya, M., 1991, "Friction Characteristics between the Piston and Cylinder for Low-Speed Conditions in a Swashplate-Type Axial Piston Motor," *J. JSME*, Vol. 57, No. 540, pp 237~241.

Murrenhoff, H. and Bebber, D. V., 2002, "Development of Coatings for Fluid Power Components for Environmentally Acceptable Pressure Media," *Proc. 13th Int. Coloquium Tribology*, Stuttgart, Germany, pp. 59~65.

N. N., 2001, "Secondary by Name But Not by Nature," *Aircraft Technology Engineering & Maintenance-April/May*, pp. 28~33.

N. N., 2003, *SKF Products Catalog*.

Olems, L., 2002, "Ein Simulationsmodell zur Beschreibung der Spaltstroemung in Axialkolben-maschinen der Schraegscheibenbauart," *Dr.-Ing. Dissertation*, TU Hamburg-Harburg.

Schoenau, G. J. and Burton, R. T., 1990, "Dynamic Analysis of a Variable Displacement Pump," *Tran. ASME*, Vol. 112, pp. 122~132.

Sutton, O., 1997, "Super Jumbos : New Systems to Boost Performance, Cut Costs," *INTERVIA , July/August*, pp. 31~33.

Tedric, A. H., 2001, *Rolling Bearing Analysis, 4th Ed.*, John Wiley & Sons, INC., pp. 540~549.

Townsend, D. P., 1992, *Dudley's Gear Handbook, 2nd Ed.*, McGraw-Hill Inc.

Zeiger, G. and Akers, A., 1985, "Torque on the Swash-Plate of an Axial Piston Pumps," *ASME J. Dynamic Systems, Measurement, and Control*, Vol. 107, pp. 220~226.